gust 1965

GEORGE C. MARSHALL SPACE FLIGHT CENTER

NATIONAL AERONAUTICS AND SPACE ADMINISTRATION

HUNTSVILLE, ALABAMA

BUREAU OF ENGINEERING RESEARCH

Progress Report No. 3

for

NASA Contract NAS8-11155

STABILITY OF SMALL PLASTIC CYLINDERS SUBJECTED TO INTERNAL PRESSURE AND AXIAL COMPRESSION

by

Thomas A. Carlton, Jr. and Gustavo A. Aramayo

BER COLLEGE OF ENGINEERING

THE UNIVERSITY OF ALABAMA 1831

UNIVERSITY OF ALABAMA

UNIVERSITY ALABAMA

Progress Report No. 3

For

NASA Contract NAS8-11155

STABILITY OF SMALL PLASTIC CYLINDERS SUBJECTED TO INTERNAL PRESSURE AND AXIAL COMPRESSION

by

Thomas A. Carlton, Jr. and Gustavo A. Aramayo

Submitted to

GEORGE C. MARSHALL SPACE FLIGHT CENTER

NATIONAL AERONAUTICS AND SPACE ADMINISTRATION

BUREAU OF ENGINEERING RESEARCH

UNIVERSITY OF ALABAMA

UNIVERSITY, ALABAMA

August 1965

STABILITY OF SMALL PLASTIC CYLINDERS SUBJECTED TO INTERNAL PRESSURE AND AXIAL COMPRESSION

by

Thomas A. Carlton, Jr. and Gustavo A. Aramayo

INTRODUCTION

The development of theoretical criteria for the buckling of monocoque and stiffened thin shell flight structures has taken place at a rapid pace under the impetus of the space program. The experimental verification of these criteria has made only limited progress. The reasons for the gap which has developed between theory and experimental verification are numerous. The use of high speed computers has made possible the rapid solution of complex shell stability equations. Thus, it has been possible to generate theoretical design data at a much faster rate than it can be experimentally verified.

Unfortunately, the idealized conditions assumed in the theoretical solutions are not realized in either model or prototype shell. In order to determine if the lack of ideal conditions in a physical model imposes a severe limitation on the use of totally theoretical design methods, an extensive experimental investigation must be undertaken.

In those cases where a particular structural configuration has been dictated by space and service requirements, both model and prototype have been constructed and tested so as to establish the practical limitations of that structure. The information gained is usually limited to the particular structure being studied and is not readily extrapolated to the general analysis of such structures.

It would be desirable to undertake a comprehensive experimental program to provide the necessary confidence in theoretical design criteria so that, at most, only limited non-destructive prototype testing would be indicated. The practicability of such a program is dependent on being able to provide a large number of suitable models at a reasonable cost. Therein lies the primary objective of this study: to determine if suitable models for experimental shell stability studies can be fabricated from commercially available sheets of cellulose acetate.

Under the terms of contract NAS8-11155, an experimental study was conducted to determine the suitability of cylindrical shells fabricated from flat sheets of cellulose acetate for verifying theories of shell stability. The unstiffened plastic cylinders were subjected to various combinations of axial compressive load and internal pressure. A total of thirty-two cylinders were fabricated. However, data were collected on only twenty-three cylinders. The remaining cylinders were either destroyed during installation in the testing machine or had initial imperfections that made them unsuitable for testing.

It was initially proposed to conduct tests using cylinders of various L/D and r/t ratios. However, the actual test program was limited to one value of L/D and three values of r/t. Limitations on the r/t ratio were due mainly to the difficulties encountered in the installation of the cylinders into the loading device.

TEST SPECIMENS

The cylindrical shell models were prepared from flat cellulose acetate sheets measuring 20 inches by 50 inches. Thicknesses used were 0.0075, 0.010, and 0.015 inches. These sheets were cut to form the projection of the external wall of the cylinders and a longitudinal seam was formed by making a lap joint and gluing with Fibestos cement. Depending upon the wall thickness of the cylinder, two different overlaps were used for the longitudinal seam. A 1/8 inch overlap was used for the cylinders of the 0.010 and 0.015 inch wall thickness and a 1/4 inch overlap was used for the cylinders having a wall thickness of 0.0075 inches. An attempt was made to fabricate cylinders with a wall thickness of 0.005 inches, but inability to fabricate suitable models precluded the continuation of this effort.

The basic dimensions of the cylinders were: Length 20 inches, diameter 15 inches, and wall thicknesses of 0.0075, 0.010, and 0.015 inches resulting in radius-to-thickness ratios of 1000, 750, and 500 respectively. Wall thickness had a variation of $\pm$ 0.002 inches as determined with a micrometer reading to the nearest 0.0005 inches. The diameter of the cylinders was within 0.05 per cent of the nominal dimension of 15 inches.

Coupons from each test cylinder were obtained in an attempt to determine the material properties of the individual specimen. Flat coupons 1 inch wide and having various gage lengths were used. The results of these tests were inconsistent and found to be of little value in determining the modulus of elasticity and Poisson's ratio.

In a further attempt to determine the material properties, data collected in the testing of the individual cylinders were analyzed. From the test of a cylinder at zero internal pressure, the modulus of elasticity

in compression can be computed from the load-deformation curve and the dimensions of the cylinder. Then, if the vertical deformation of the unstrained cylinder is totally restrained when the internal pressure is applied, i.e., $\epsilon_y = 0$, it is possible to compute Poisson's ratio. When the cylinder is clamped to the loading head, the difference between the internal pressure force on the loading head and the load required to prevent vertical deformation in the cylinder is used to compute the longitudinal tensile stress, σ_y, in the cylinder wall. The hoop stress, σ_x, is equal to $p(r/t)$. Thus, Poisson's ratio, ν, is σ_y/σ_x. However, measured forces indicated that slipping occurred between the cylinder and the loading head in every test, thus, partially relieving the induced σ_y stress. For this reason, it was necessary to disregard calculated values of Poisson's ratio and use an assumed value of 0.3. From the results of the tension tests of the coupons, the test cylinder data and manufacturer's recommendations, a modulus of elasticity of 4×10^5 p.s.i. was assumed.

EQUIPMENT AND PROCEDURES

An Instron universal testing machine was used for applying the load and measuring the load and deformation. The deformation measured was the total movement of the machine platen and included any slipping between the loading head and the test cylinder. The load was transferred to the cylinders by means of end loading plates. The plates were designed to fit into the test cylinder a distance of one inch. The lower plate was fastened to the movable head of the machine and the upper plate was fastened to a load cell. The cylinders were installed in the loading rig by sliding the ends of the specimen over the loading plates and then clamping to the loading plates with a metal strap one-half inch wide. Thus, the load was transferred through the clamps into the cylinder. The clamps also helped seal any pressure leaks resulting from a lack of fit between the cylinder and the loading plates.

Internal pressure was provided from an air supply at 150 p.s.i. The air passed through a pressure regulator and a relief valve before going into the cylinder. A constant pressure was maintained during each test by allowing a regulated amount of air to escape from the cylinder. Internal pressure was measured by means of a manometer reading in inches of mercury. Load versus deformation was obtained from an X - Y recorder with an electric strain gage load cell providing the load input and a resistance potentiometer providing machine crosshead movement as the deformation input.

The cylinder specimens were deformed at a constant rate. In order to determine the effect of rate of loading on the critical buckling load, two different rates were investigated. These rates were 0.005 and 0.05

inches/minute displacement of the crosshead of the loading machine. At low values of internal pressure, the buckling load resulting from the high rate of deformation was about 3 per cent higher than the buckling load obtained using the lower rate. However, at values of internal pressure of 1.5 p.s.i. and higher, no difference in the buckling loads was found at the two different rates of deformation. The data collected represent values of buckling corresponding to the slow rate of loading.

The load-deformation curve for the test cylinders was essentially linear over most of the range. However, near the maximum load, a sharp but smooth transition into a horizontal plateau of constant load and increasing deformation occurred. Critical buckling load was determined from this horizontal plateau of the load-deformation curve.

In some cases, the formation of isolated diamond-shaped buckles occurred prior to any indication of buckling in the load-deformation curve. The load at which this occurred was not recorded since the critical buckling load was found to be only slightly higher. The formation of buckles in the unpressurized cylinders was predominant around the seam in regions that showed some initial imperfections. At higher loads, the buckles showed a more uniform distribution and they were always more numerous in areas having such initial imperfections as dents and ripples.

In the pressurized cylinder tests, the internal pressure eliminated most of the visible evidence of imperfections in the cylinders. In the pressurized tests, the formation of the diamond-shaped buckles was preceded by the formation of a uniform circumferential ripple at top and bottom of the specimen. At the critical buckling load established by the load-deformation curve, some diamond shape buckles appeared in the same regions and progressed in the circumferential direction. These buckles, in contrast with the ones formed in unpressurized tests, had

their maximum dimension in the circumferential direction.

The tests were conducted by first applying the internal pressure to the cylinder while preventing any movement of the testing machine platen. The restraining force was recorded. The axial compressive load was then applied to the cylinder while the internal pressure remained constant. Each cylinder was subjected to a series of tests in which the internal pressure was varied from test to test and in which the cylinder was ultimately destroyed. After a cylinder was buckled at one value of internal pressure, the load and pressure were relieved, the pressure was increased by 1/2 psi and the cylinder was again loaded to the critical buckling load at the increased internal pressure. This procedure was established after one cylinder was tested to determine if it were possible to re-use the same cylinder for different values of internal pressure. Preliminary tests showed that the same cylinder could be used several times provided that the deformation was stopped as soon as the critical buckling load was reached.

THEORETICAL BUCKLING CRITERION

A summary of the theoretical buckling criteria for pressurized and unpressurized monocoque thin shells is presented by Harris, Suer, Skene, and Benjamin. (1) Critical buckling stress for the unpressurized cylinder based on Donnell's (2) equations is given in terms of a buckling coefficient, K_c. For the case of unpressurized long cylinders, this theoretical buckling coefficient becomes

$$K_c = \frac{4\sqrt{3}}{\pi^2}\left(\frac{L^2}{rt}\right)\sqrt{1-\nu^2} \tag{1}$$

The equation for critical stress is

$$\frac{\sigma_{cr}}{\eta} = K_c \pi^2 D \left(\frac{t}{L}\right)^2 \tag{2}$$

Substitution of the buckling coefficient into the critical stress equation results in the following equation for critical stress

$$\frac{\sigma_{cr}}{\eta} = \left(\frac{E}{\sqrt{3(1-\nu^2)}}\right)\left(\frac{t}{r}\right) \tag{3}$$

where $\eta = 1$ for the case of elastic buckling.

For a cylinder subjected to a combination of axial load and internal pressure, the critical stress and internal pressure are expressed in terms of the following non-dimensional parameters.

$$\bar{\sigma}_{cr} = \frac{\sigma_{cr}}{E}\left(\frac{r}{t}\right) \tag{4}$$

$$\bar{p} = \frac{p}{E}\left(\frac{r}{t}\right)^2 \tag{5}$$

where σ_{cr} is the stress in the cylinder at buckling.

Lo, Crate, and Schwartz (3) indicate that this stress is equal to the stress in the cylinder corresponding to the load in the cylinder at

the time of local buckling in any particular region of the shell. Thus, from these parameters and in accordance with Lo's analysis, the value of $\bar{\sigma}_{cr}$ increases from 0.376 for $\bar{p} = 0$ to a maximum of 0.605 for $\bar{p} = 0.169$. The Flugge theory (4) indicates that the value of $\bar{\sigma}_{cr}$ is equal to 0.605 for all values of $\bar{p}$.

Following Lo's analysis, another non-dimensional parameter,

$$\Delta\bar{\sigma}_{cr} = \bar{\sigma}_{cr} - \bar{\sigma}_{cro} \tag{6}$$

can be determined. The only new term is $\bar{\sigma}_{cro}$, the non-dimensional stress corresponding to a condition of zero internal pressure. The definition of the stress term is the same as the one indicated for the non-dimensional buckling stress. Test results can be interpreted as a per cent of the theoretical buckling stress computed by equation 3. Both the theoretical and experimental buckling stress and the internal pressures are substituted into equations 4 and 5 for comparison purposes.

In the analysis of the unpressurized cylinders, equation 1 is rewritten in the following form

$$K_c = \frac{4\sqrt{3}}{\pi^2} (Z) \tag{7}$$

where the value of Z is as follows:

$$Z = \frac{L^2}{rt}\sqrt{1 - \nu^2} \tag{8}$$

Also, equation 4 is rewritten in the following form:

$$\sigma_{cr} = E\ \bar{\sigma}_{cr}\left(\frac{t}{r}\right) \tag{9}$$

EXPERIMENTAL DATA

The results of the experimental study are presented in Tables I, II, III, and IV of the appendix. For ease in analysis, these data are further summarized in graphical form. The experimental data have been substituted into equations 4 and 5 and the results plotted in Figures 1, 2, and 3. Each of these figures presents the data for a particular value of r/t. The critical buckling stress, σ_{cr}, was computed as the net buckling load divided by the cross-sectional area of the cylinder wall. The net buckling load is the total load on the cylinder at buckling minus the internal pressure reaction load, $p(\pi r^2)$. Each of the above figures contains all of the satisfactory experimental values of $\bar{\sigma}_{cr}$ vs $\bar{p}$ for a particular r/t ratio. In addition, the values of $\bar{\sigma}_{cr}$ have been averaged for each value of $\bar{p}$ and a curve sketched for these average values of $\bar{\sigma}_{cr}$. The theoretical relationship according to Lo (3) is also shown on each of these figures. It should be noted that the experimental data more closely approximates the theory for the highest r/t ratio of 1000. The average values, taken from Figures 1, 2, and 3, have been summarized in Figure 4 for comparison purposes.

The data of Tables 1, II, and III have also been substituted into equation 6 and the results plotted in Figures 5, 6, and 7. Average values from these graphs are summarized in Figure 8. These figures emphasize the stabilizing influence of internal pressure. Lo, Crate, and Schwartz (3) have suggested that better correlation between theory and experiment can be obtained if the increment in buckling parameter, $\Delta\bar{\sigma}_{cr}$, is plotted against the pressure parameter, $\bar{p}$.

The experimental data for the unpressurized cylinders are presented in Figure 9 as a plot of the stress parameter, $\bar{\sigma}_{cr}$, versus the r/t ratio. A best fit curve for these data was determined by the method of least squares. The equation for this curve is as follows:

$$\bar{\sigma}_{cr} = 0.209 - 0.00003 \frac{r}{t} \qquad (10)$$

Using equation 10, for r/t ratios of 500, 750, and 1000, values of $\bar{\sigma}_{cr}$ were computed respectively as 0.194, 0.186, and 0.179. It follows then, from equation 9, that, for the unpressurized cylinders, the best fit experimental values of the critical buckling stress, σ_{cr}, are respectively 155.00, 99.20, and 71.60 p.s.i. Equation 2 was solved for the buckling coefficient, K_c, for the case of elastic buckling and the materials and geometry used in this study. The values of the buckling coefficient, K_c, are respectively $(4.438)(\sigma_{cr})$, $(9.9855)(\sigma_{cr})$, and $(17.752)(\sigma_{cr})$ for r/t ratios of 500, 750, and 1000. Using the values of critical buckling stress, σ_{cr}, computed above, the experimental buckling coefficients, K_c, become respectively 687.89, 990.56, and 1271.04. The values of Z computed from equation 8 are 3060, 4591, and 6120 for wall thicknesses of 0.015, 0.010, and 0.0075, respectively.

The values of experimental K_c and Z computed above have been plotted on log-log paper in Figure 10 after the manner of Harris, Suer, Skene, and Benjamin (1). Superimposed on this plot are the theoretical and the 90 per cent probability curves taken from the same reference.

ANALYSIS OF RESULTS

The fabrication of the test cylinders was performed in a very unsophistocated manner. The sheets were hand trimmed and the cylinders were not formed around a mandrel. Rather, the joints were formed on a flat table such that the original specimen looked more like an envelop than a cylinder. This resulted in a test specimen in which small local imperfections were readily noticeable. Unfortunately, it is not possible to represent the quality of the specimen in terms of initial local imperfections. However, it must be assumed that all had some local imperfections.

In view of the above observations on local imperfections, several interesting observations can be made from Figures 1, 2, and 3. It can be observed that, for all three r/t ratios represented in these figures, the curve for the average values tends to flatten out and become parallel to the theoretical curve of Lo as $\bar{p}$ increases. Furthermore, the experimental scatter tends to lessen as $\bar{p}$ increases. Since the same cylinders were used in most cases for the full range of $\bar{p}$, it appears that the effect of local imperfections is less at high pressures. This is slightly misleading since many of the highly imperfect cylinders were actually destroyed before the higher values of internal pressure could be reached.

Assuming that the scatter in the experimental data is directly related to the quality of the cylinder, it is obvious that a large number of tests must be conducted when relatively imperfect cylinders are used. Although the behavior of the individual models is erratic, the curves representing the averages of the several tests behave very much according to theory. An error in the modulus of elasticity would shift all data points an equal relative amount, but the scatter is strictly a function

of the models and of the testing procedure and the trend of the averages is a measure of the ability of cellulose acetate to serve as a material from which to construct the models.

Another interesting observation can be made concerning the effect of initial imperfections as a function of r/t ratio. In Figure 1, for r/t of 500, the scatter is large and the trend of the averages is irregular. In Figure 2 for r/t of 750, the trend of the averages is smoother and more closely approaches the theoretical curve. In Figure 3, for r/t of 1000, the trend of the averages is quite smooth and indicates that the behavior of the cylinders can be approximated by the theory of Lo. Thus, it appears that, when pressurized, test data for the cylinders having the higher r/t ratios, or at least made from the thinner materials, are less effected by the initial imperfections. This assumes that models of all thicknesses had the same relative initial imperfections.

According to Lo, Crate, and Schwartz (3), a better correlation between theory and experiment can be obtained if the increment in buckling parameter, $\Delta \bar{\sigma}_{cr}$, as computed by equation 6, is plotted against the pressure parameter, $\bar{p}$. This appears to be verified by the results shown in Figure 5 for the cylinders having an r/t of 500. However, Figures 6 and 7 for the higher r/t ratios show the data points to fall well above the theory line of Lo. In attempting to verify the theory, Lo assumed that the unpressurized buckling parameter, $\bar{\sigma}_{cro}$, was always equal to 0.36, and subtracted this value from the experimental pressurized buckling parameter, $\bar{\sigma}_{cr}$, to obtain the incremental buckling parameter, $\Delta \bar{\sigma}_{cr}$. However, from Figures 1, 2, and 3 it is seen that the unpressurized buckling parameter, $\bar{\sigma}_{cro}$, determined in the experimental program at the University of Alabama is of the order of 0.2. Had the theoretical un-

pressurized buckling parameter, 0.36, been used to compute the points shown in Figures 6 and 7, the results would have very closely approximated the theory of Lo. To a lesser extent, the same would have been true for the higher values of $\bar{p}$ shown in Figure 5. Thus, it is clearly seen that the effects of pressurization quickly minimize the influence of model imperfections on the buckling strength of cylinders made with thinner materials. Also, at higher pressures, the thicker materials are less influenced by the initial imperfections. The theory of Lo appears to be satisfactory for determining the critical buckling strength of high r/t, pressurized cylinders and for lower r/t cylinders having high internal pressures.

The critical buckling parameter, $\bar{\sigma}_{cr}$, of the unpressurized cylinders has been plotted against r/t in Figure 9, and a best fit curve determined by least squares. The values of $\bar{\sigma}_{cr}$ determined from this curve together with the respective r/t ratios was used to compute values of K_c and Z from equations 2 and 8 respectively. These values have been plotted in Figure 10 against the theoretical curve of these quantities and the 90 per cent probability curve. It is noted that, in each case, the results determined from the best fit line fall above the 90 per cent probability line. Furthermore, in only two cases do the individual test results fall below the 90 per cent probability line.

CONCLUSIONS

The limited nature of the experimental work performed in this investigation does not permit reaching a large number of broad conclusions. However, within the scope of the work performed, several limited but important conclusions can be drawn.

1. The large amount of scatter in the test results indicates that more care should be taken in fabricating the test specimens and in conducting the individual tests. Several nearly identical specimens should be tested and the average of the results used for analysis purposes.

2. The manner in which the data obtained using cylinders fabricated from cellulose acetate tend to verify the theory of Lo, Crate, and Schwartz (3), indicates that the use of this material for providing low cost test cylinders should be encouraged. However, a satisfactory method of determining the modulus of elasticity must be used.

3. For cylinders having high r/t ratios, the effect of initial local imperfections on buckling strength is quickly minimized by internal pressure. The more rigid the walls of the cylinder, the higher must be the internal pressure to satisfactorily minimize the imperfections.

4. In studying unpressurized cylinders, the test specimens should be as nearly free of initial imperfections as possible. The presence of such imperfections critically influences the buckling strength of such cylinders.

5. The theory of Lo, Crate, and Schwartz (3) is satisfactory for determining the critical buckling strength of pressurized unstiffened cylinders provided that the walls behave as a membrane.

6. Test cylinders of cellulose acetate can be buckled elastically several times without materially effecting the critical buckling load. This is true for both the pressurized and the unpressurized conditions.

REFERENCES

1. Harris, A. L.; Herbert, S. S.; Skene, W. T.; and Benjamin, R. J.: The Stability of Thin-Walled Unstiffened Cylinders Under Axial Compression Including Effects of Internal Pressure. Journal of the Aeronautical Sciences, Vol. 24, No. 8, August 1957., p. 587.

2. Batdorf, S. B.: A Simplified Method of Elastic-Stability Analysis for Thin Cylindrical Shells. NACA Rept. 874, 1947.

3. Lo, H.; Crate, H.; and Schwartz, E. B.: Buckling of Thin Walled Cylinders Under Axial Compression and Internal Pressure. NACA Report 1027, 1951.

4. Flugge, W.: Die Stabilitat Der Krieszylinderschale. Ing-Archiv, Bd. III, Heft 5, December, 1932, pp. 463-506.

TABLE I. - TEST RESULTS FOR CYLINDERS WITH r/t of 500.

Specimen Number	p	$\bar{p}$	P_{cr}	σ_{cr}	$\bar{\sigma}_{cr}$	$\Delta\bar{\sigma}_{cr}$
15	0	0	120.0	169.76	0.211	0
24	0	0	99.0	140.05	0.175	0
28	0	0	108.0	152.78	0.191	0
29	0	0	130.0	183.91	0.230	0
30	0	0	133.0	188.15	0.235	0
15	1	0.625	223.3	315.90	0.395	0.184
24	1	0.625	171.3	242.34	0.303	0.128
28	1	0.625	233.3	330.05	0.413	0.222
29	1	0.625	250.3	354.10	0.443	0.213
30	1	0.625	253.3	358.34	0.448	0.213
15	2	1.250	186.6	263.98	0.330	0.119
24	2	1.250	166.6	235.67	0.294	0.119
28	2	1.250	256.6	363.01	0.454	0.263
29	2	1.250	256.6	363.01	0.454	0.224
30	2	1.250	259.6	367.26	0.459	0.224
15	3	1.875	172.9	244.60	0.305	0.094
24	3	1.875	144.9	204.99	0.256	0.081
28	3	1.875	314.9	445.49	0.557	0.366
29	3	1.875	270.9	383.24	0.479	0.249
30	3	1.875	264.9	374.75	0.468	0.233
24	4	2.500	133.2	188.44	0.236	0.061
28	4	2.500	293.2	414.79	0.518	0.327
29	4	2.500	271.2	383.67	0.479	0.249
30	4	2.500	263.2	372.35	0.465	0.230
28	5	3.125	271.5	384.09	0.480	0.289
29	5	3.125	321.5	454.83	0.568	0.338
28	6	3.750	249.8	353.39	0.442	0.251
29	6	3.750	299.8	424.13	0.530	0.300

TABLE II. - TEST RESULTS FOR CYLINDERS WITH r/t of 750.

Specimen Number	p	$\bar{p}$	P_{cr}	σ_{cr}	$\bar{\sigma}_{cr}$	$\Delta\bar{\sigma}_{cr}$
6	0	0	51	108.24	0.202	0
7	0	0				
8	0	0	52	110.36	0.207	0
9	0	0	30	63.67	0.119	0
14	0	0	41	87.02	0.163	0
16	0	0	25	53.06	0.099	0
21	0	0	43	91.26	0.171	0
22	0	0				
6	1	1.406	95.3	202.27	0.379	0.177
7	1	1.406	113.3	240.47	0.451	
8	1	1.406	113.3	240.47	0.451	0.244
9	1	1.406	131.3	278.67	0.521	0.402
14	1	1.406	118.3	251.08	0.471	0.308
16	1	1.406	104.3	221.37	0.415	0.316
21	1	1.406	136.3	289.28	0.289	0.118
22	1	1.406	114.3	242.59	0.455	
7	2	2.812	107.6	228.37	0.428	
9	2	2.812	146.6	311.15	0.583	0.464
14	2	2.812	141.6	300.53	0.563	0.400
16	2	2.812	126.6	268.70	0.504	0.405
21	2	2.812	139.6	296.29	0.555	0.384
22	2	2.812	113.6	241.11	0.452	
7	3	4.218	111.9	237.50	0.445	
9	3	4.218	162.9	345.74	0.648	0.529
14	3	4.218	126.9	269.34	0.505	0.342
16	3	4.218	124.9	265.09	0.497	0.398
21	3	4.218	129.9	275.70	0.517	0.346
22	3	4.218	116.9	248.11	0.465	

TABLE II. - TEST RESULTS FOR CYLINDERS WITH r/t of 750-CONCLUDED.

Specimen Number	p	$\bar{p}$	P_{cr}	σ_{cr}	$\bar{\sigma}_{cr}$	$\Delta\bar{\sigma}_{cr}$
7	4	5.625	153.2	325.15	0.609	
9	4	5.625	133.2	287.70	0.530	0.411
14	4	5.625	133.2	282.70	0.530	0.367
21	4	5.625	148.2	314.54	0.589	0.418
22	4	5.625	138.2	293.32	0.550	
7	5	7.031	126.5	268.48	0.503	
21	5	7.031	141.5	300.32	0.563	0.392
22	5	7.031	141.5	300.32	0.563	

Note: Values of $\Delta\bar{\sigma}_{cr}$ are not given for cylinders 7 and 22 since tests were not conducted on these cylinders in the unpressurized condition.

TABLE III. - TEST RESULTS FOR CYLINDERS WITH r/t of 1000.

Specimen Number	p	$\bar{p}$	P_{cr}	σ_{cr}	$\bar{\sigma}_{cr}$	$\Delta\bar{\sigma}_{cr}$
11	0	0				
17	0	0				
18	0	0				
26	0	0	21	59.42	0.148	0
31	0	0	31	87.72	0.219	0
32	0	0	31	87.72	0.219	0
11	1	2.50	88.3	249.8	0.624	
17	1	2.50	68.3	193.26	0.483	
18	1	2.50	48.3	136.67	0.342	
26	1	2.50	83.3	235.71	0.589	0.441
31	1	2.50	83.3	235.71	0.589	0.370
32	1	2.50	97.3	275.32	0.688	0.469
11	2	5.00	66.6	188.45	0.471	
17	2	5.00	73.6	208.25	0.521	
18	2	5.00	74.6	211.09	0.528	
26	2	5.00	91.6	259.19	0.649	0.501
31	2	5.00	91.6	259.19	0.647	0.428
32	2	5.00	94.6	267.68	0.669	0.450
17	3	7.50	79.9	226.08	0.565	
18	3	7.50	79.9	226.08	0.565	
26	3	7.50	87.9	248.72	0.622	0.474
31	3	7.50	74.9	211.94	0.530	0.311
32	3	7.50	97.9	277.02	0.693	0.474
17	4	10.0	83.2	235.42	0.588	
32	4	10.0	78.2	211.27	0.553	0.334

Notes: 1. In Tables I, II and III, P_{cr} is expressed in pounds; σ_{cr} and p are expressed in psi; $\bar{p}$, $\bar{\sigma}_{cr}$ and $\Delta\bar{\sigma}_{cr}$ are dimensionless.

2. Unpressurized tests were not conducted on cylinders 11, 17, 18.

TABLE IV. - TEST RESULT AVERAGES

p	$\bar{p}$	r/t	$\bar{\sigma}_{cr}$	$\Delta\bar{\sigma}_{cr}$
0	0	500	0.208	0
1	0.625	500	0.400	0.192
2	1.250	500	0.398	0.190
3	1.875	500	0.413	0.205
4	2.500	500	0.425	0.217
5	3.125	500	0.524	0.316
6	3.750	500	0.486	0.276
0	0	750	0.160	0
1	1.406	750	0.429	0.261
2	2.812	750	0.514	0.413
3	4.218	750	0.513	0.404
4	5.625	750	0.562	0.399
5	7.031	750	0.543	0.392
0	0	1000	0.195	0
1	2.50	1000	0.553	0.427
2	5.00	1000	0.581	0.460
3	7.50	1000	0.595	0.420
4	10.00	1000	0.571	0.334

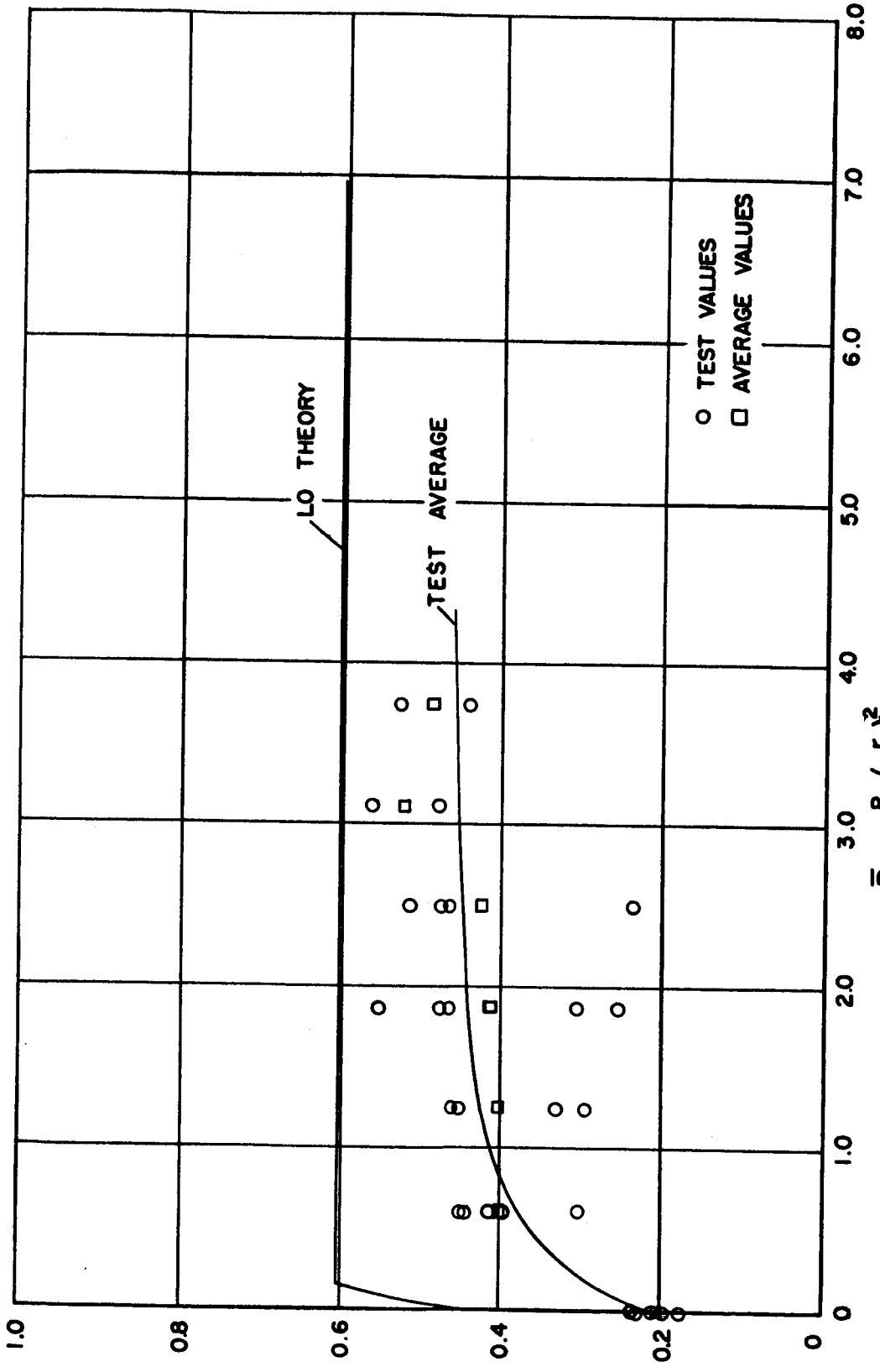

FIGURE 1 - TEST RESULTS FOR CYLINDERS WITH 1/4 OF 500

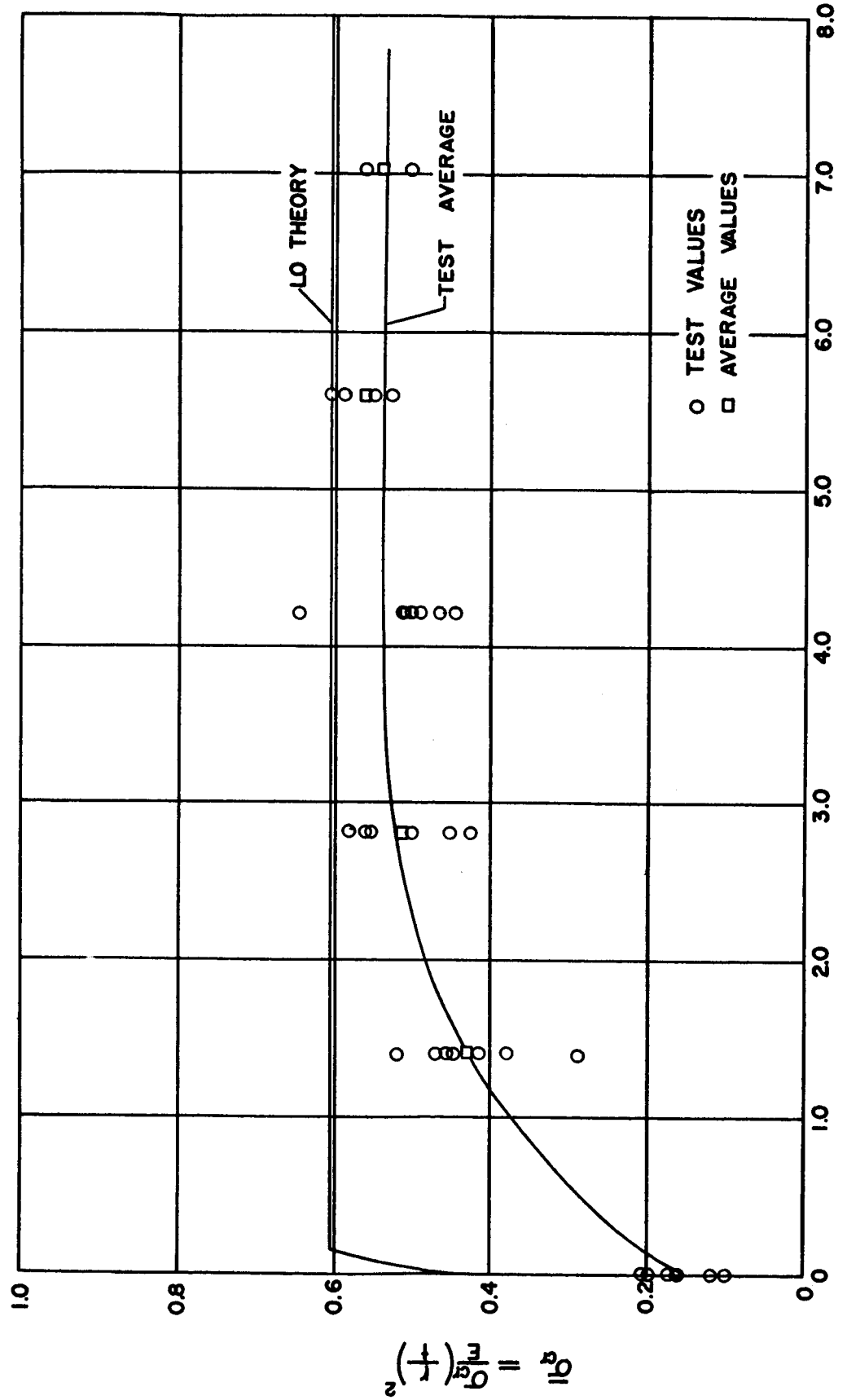

FIGURE 2 – TEST RESULTS FOR CYLINDERS WITH r/t OF 750

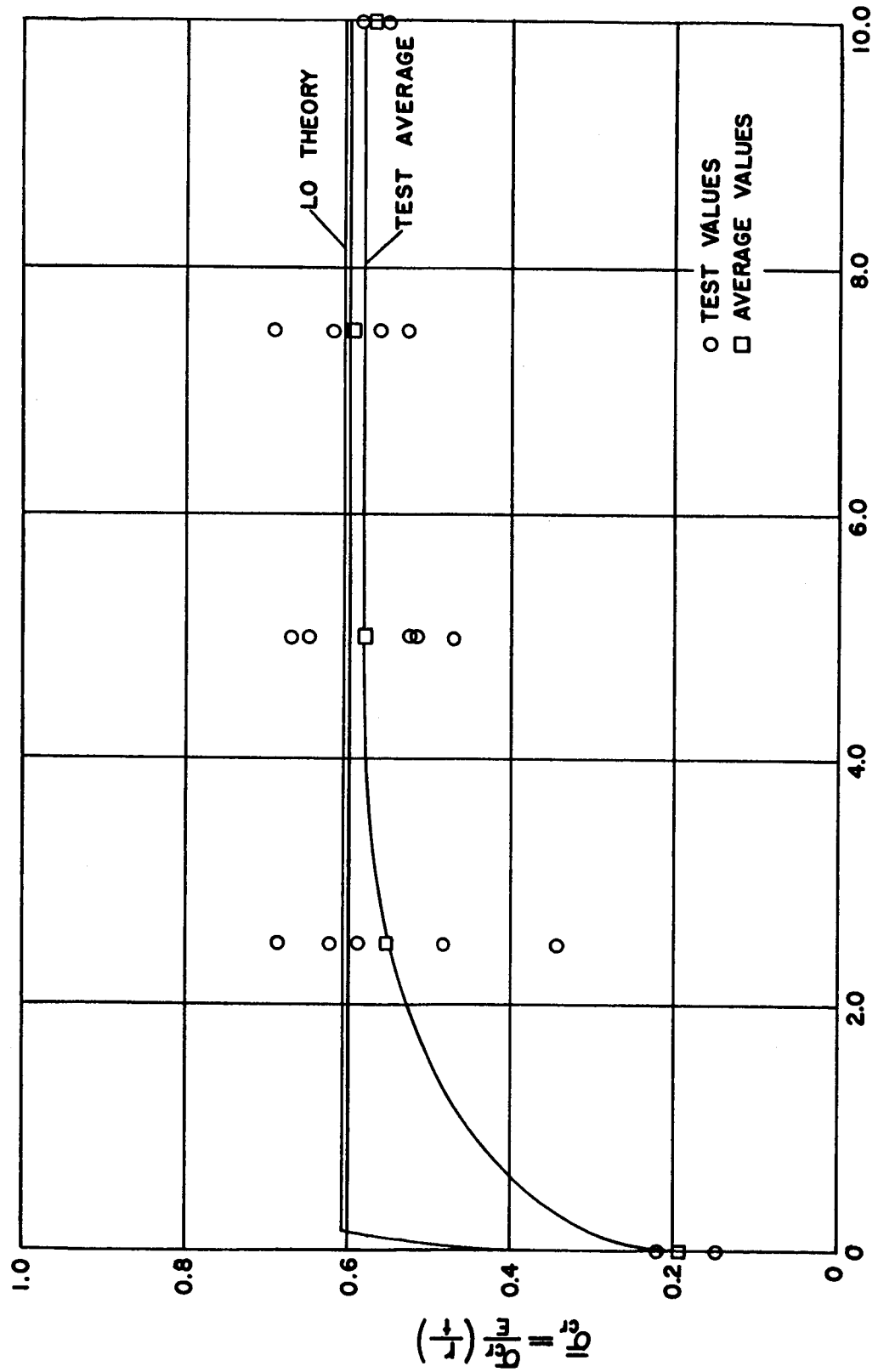

FIGURE 3 — TEST RESULTS FOR CYLINDERS WITH r/t OF 1000

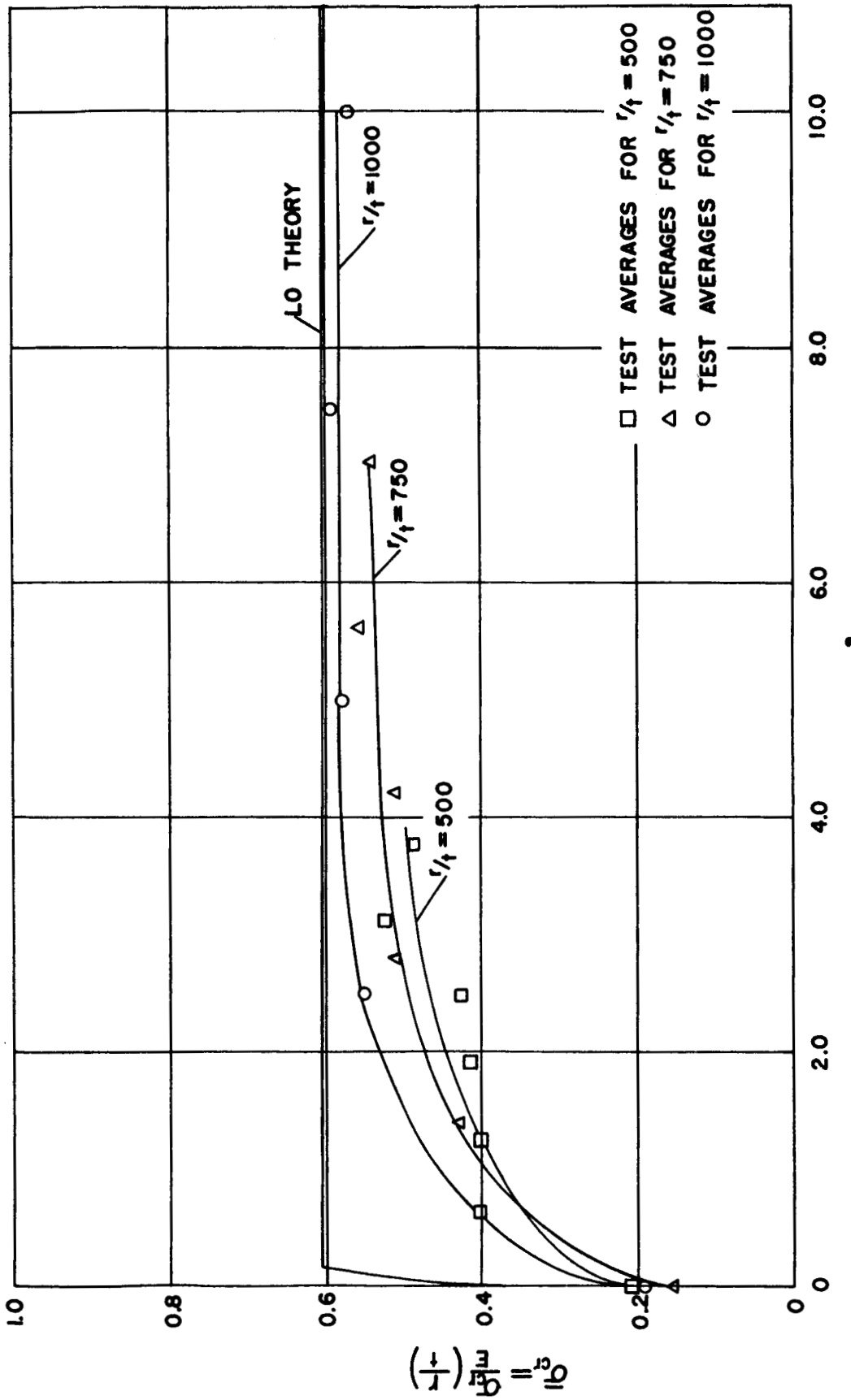

FIGURE 4 — SUMMARY OF AVERAGE TEST VALUES

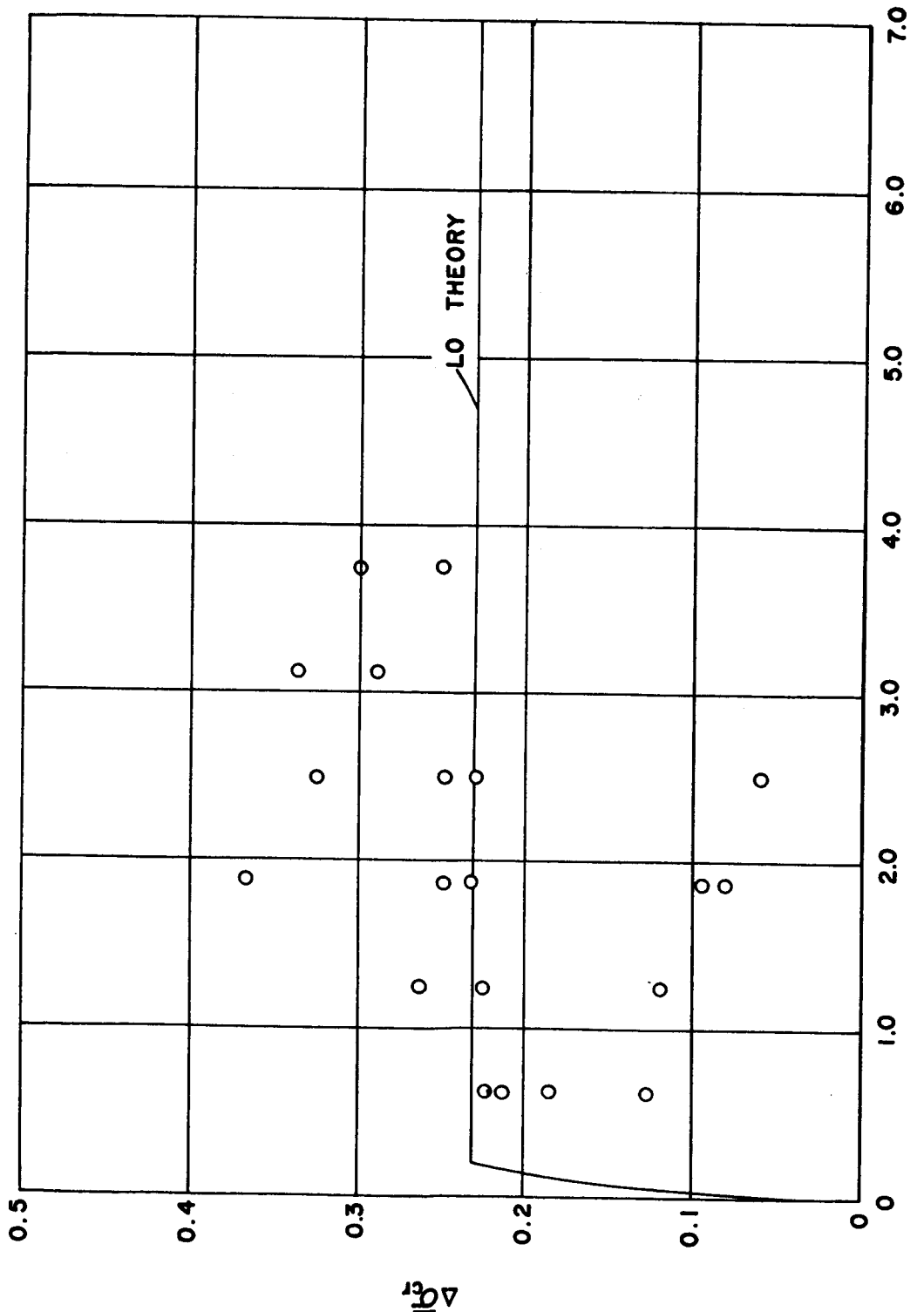

FIGURE 5 – TEST VALUES OF $\Delta\bar{\sigma}_{cr}$ FOR r/t OF 500

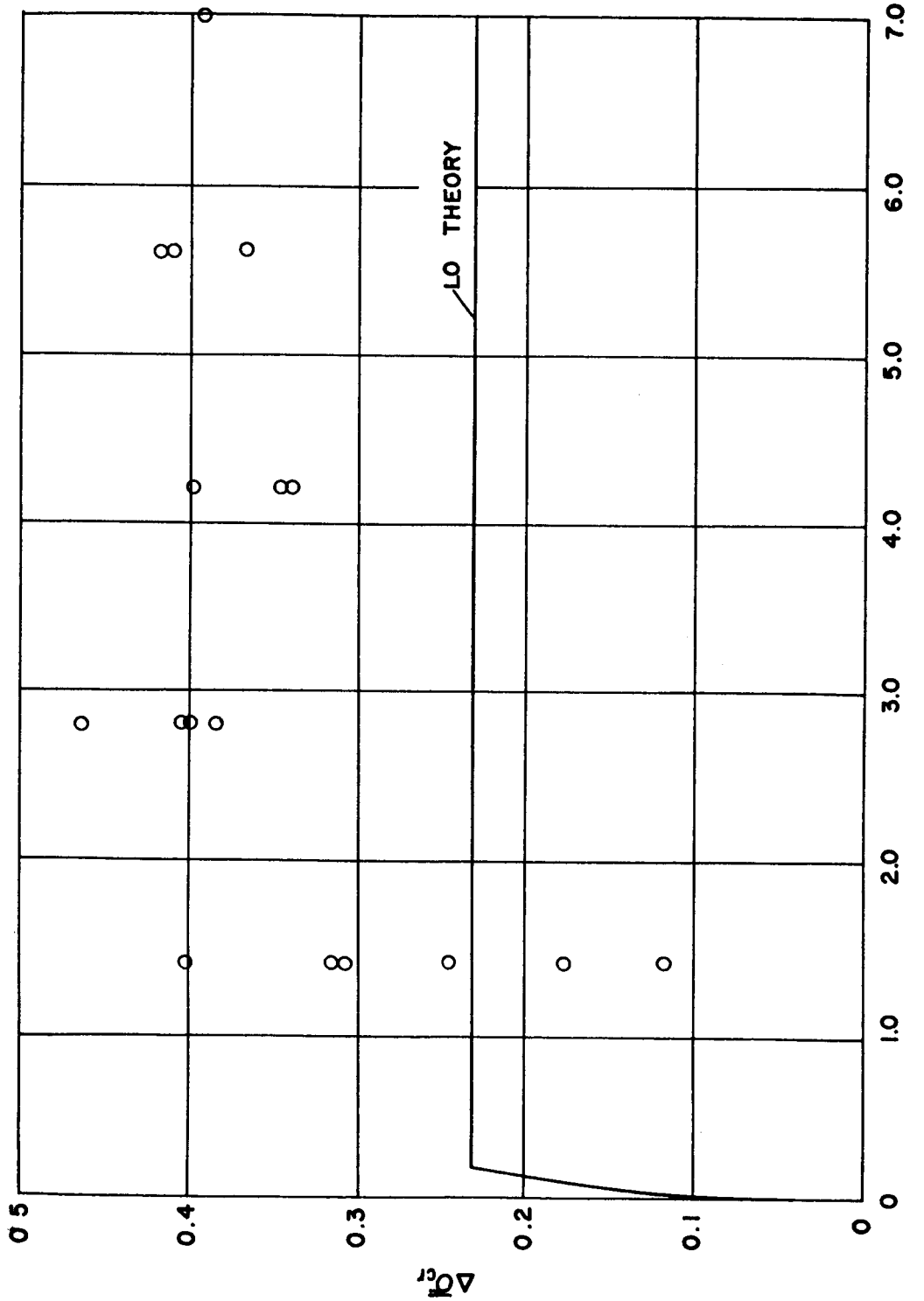

FIGURE 6 – TEST VALUES OF $\Delta\bar{\sigma}_{cr}$ FOR r/t OF 750

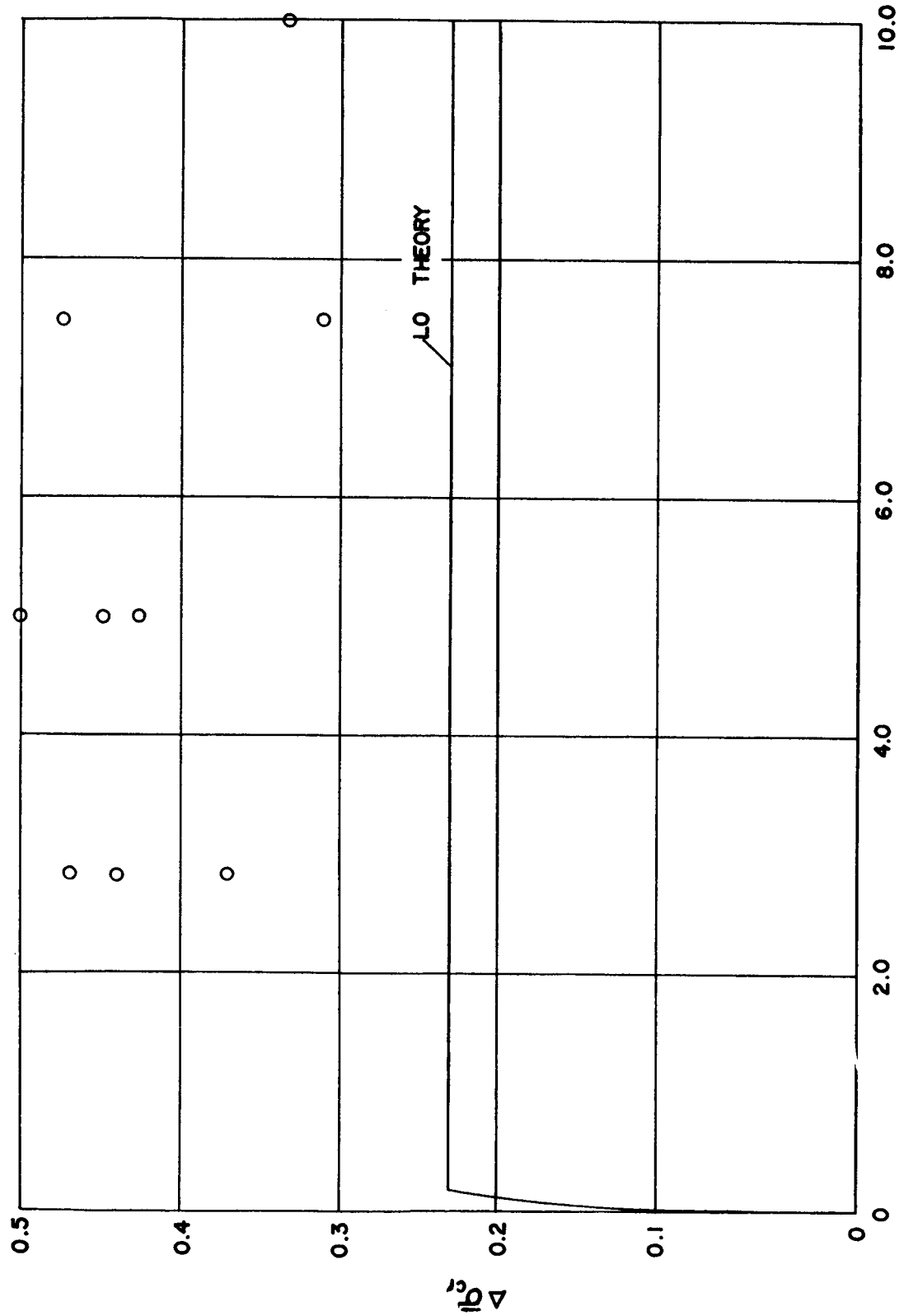

FIGURE 7 – TEST VALUES OF $\Delta\bar{\sigma}_{cr}$ FOR r/t OF 1000

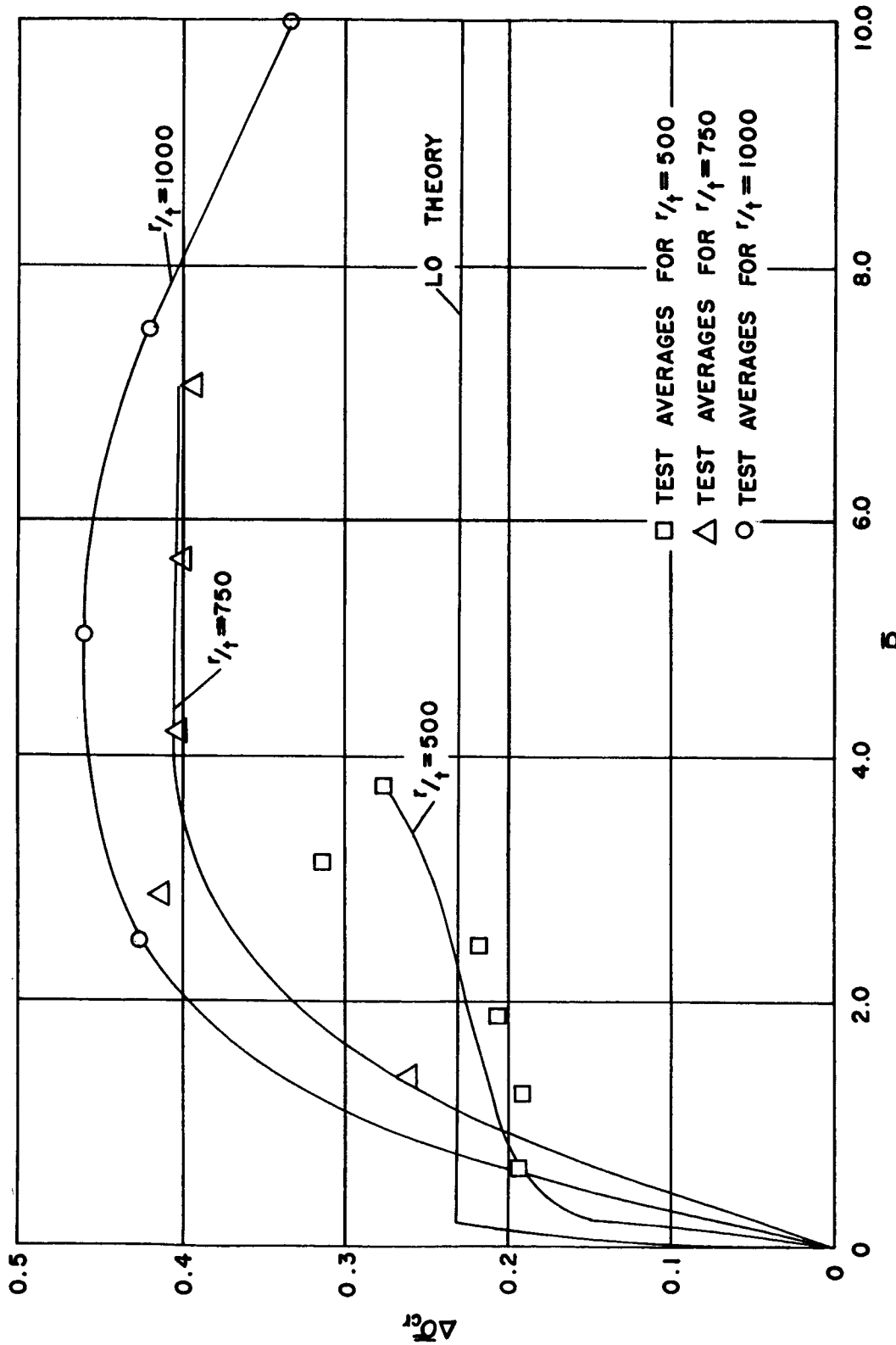

FIGURE 8 – AVERAGE VALUES OF $\Delta\bar{\sigma}_{cr}$

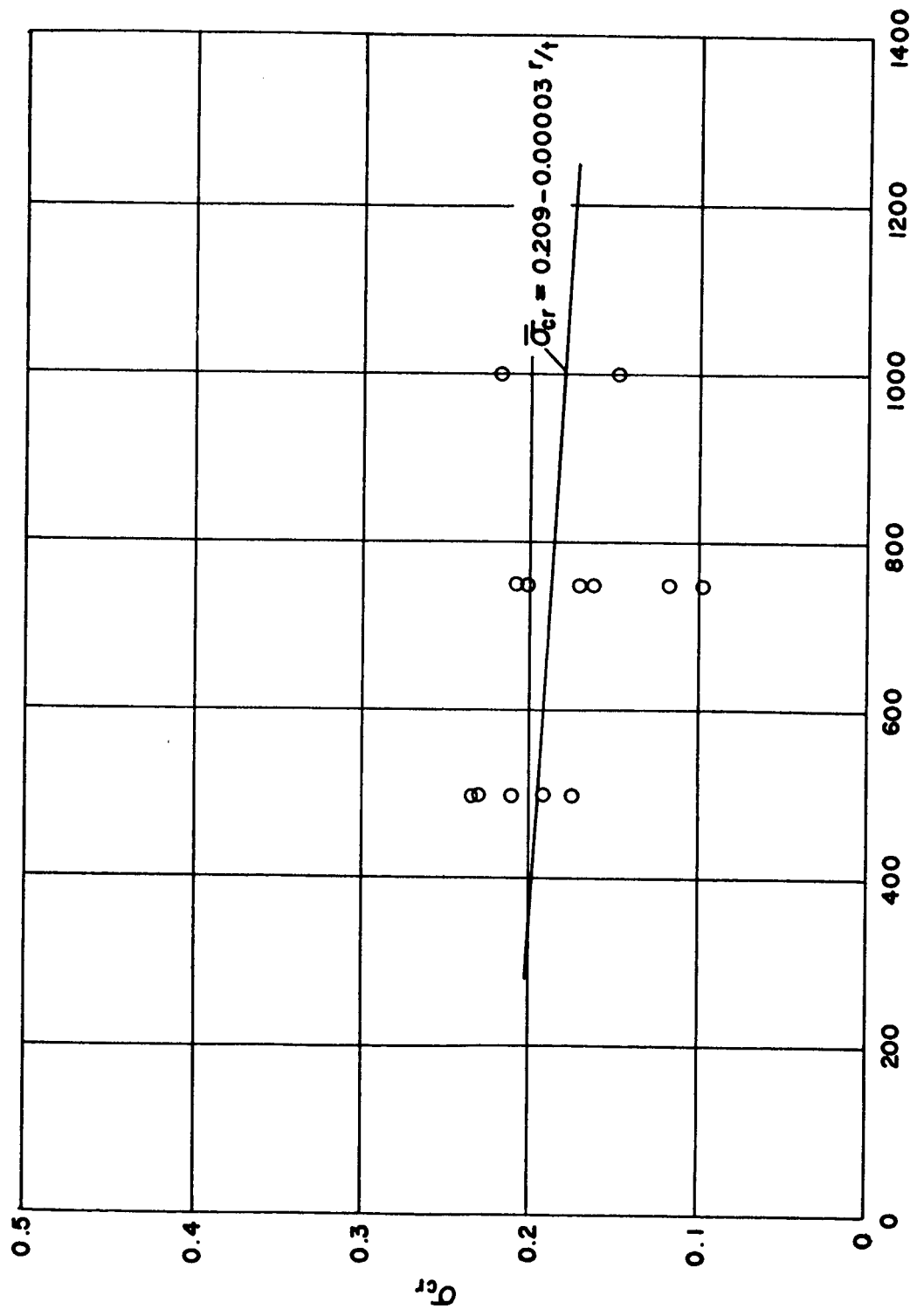

FIGURE 9 – BEST FIT CURVE FOR UNPRESSURIZED CYLINDERS

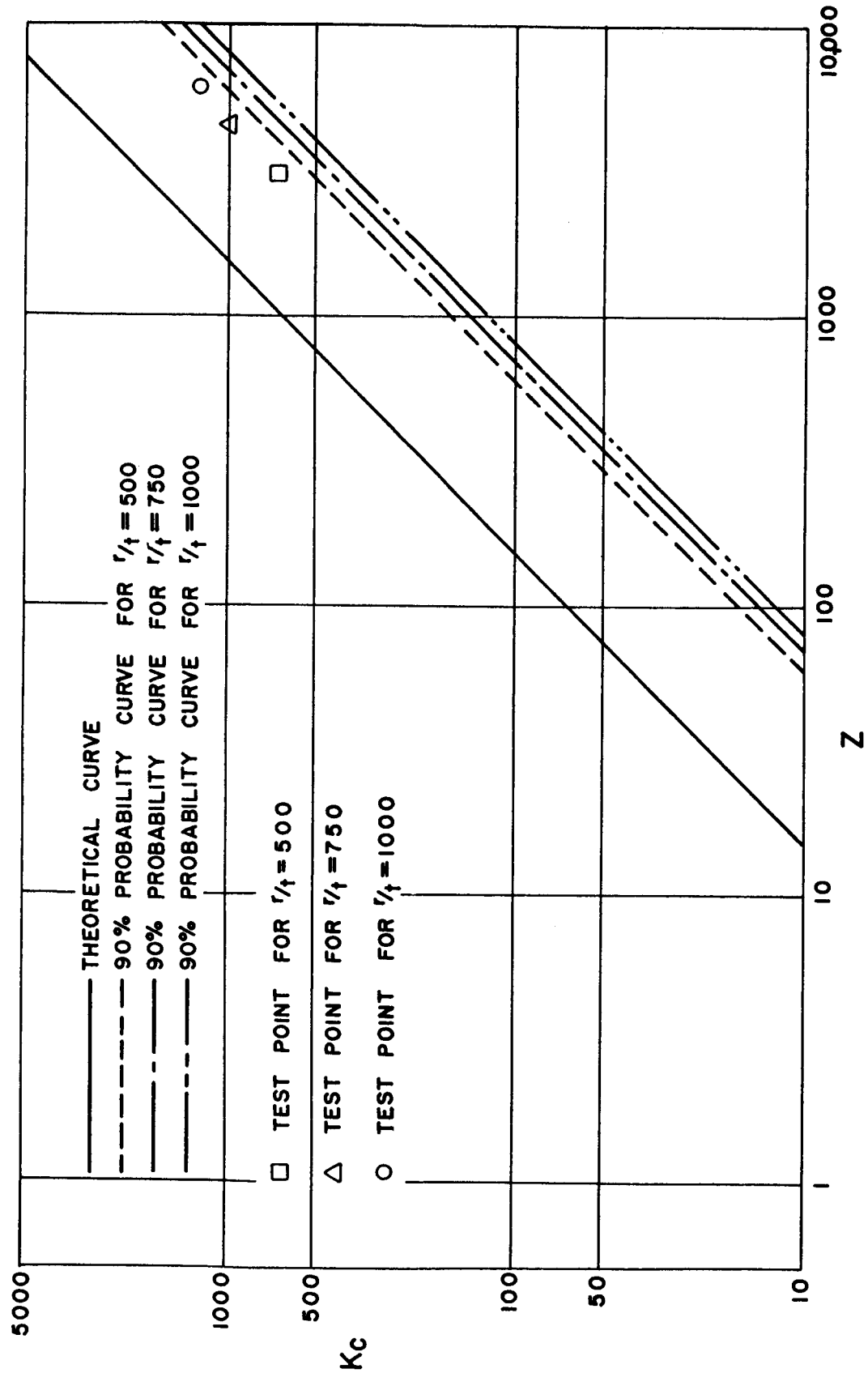

FIGURE 10 – BUCKLING COEFFICIENT, K_c, FOR UNPRESSURED CYLINDERS